BISTATIC MICROWAVE DIVERSITY IMAGERY

Tah–Hsiung Chu* and Ding–Bing Lin
Electrical Engineering Department, National Taiwan University
Taiwan, Republic of China

I. Introduction

Microwave imaging system finds its application in the areas of radar, nondestructive evaluation and biological diagnosis etc., because microwaves can penetrate fog, cloud, dust and a variety of dielectric materials. In this paper, derivation of the microwave image reconstruction scheme for objects (either perfectly conducting or dielectric object) in a bistatic scattering arrangement using frequency and angular diversity techniques is presented.

II. Theoretical Development

Considering a two–dimensional scattering object, shown in Fig.1(a) and (b) is illuminated by a normally incident TM–polarized plane wave. The scattered field over a linear array located at $z=d$ (forward scattering) and $z=-d$ (backward scattering) for a perfectly conducting object satisfying the physical optics approximation is given as [1]

$$\vec{E}_s^c(x,z=\pm d,\vec{k}_0)=-j\omega\mu_0\int_{C_{ill}} 2\hat{n}\times\vec{H}_i G(|\vec{r}-\vec{r}'|)d\vec{r}' \tag{1}$$

where C_{ill} is the illuminated object contour, $\hat{n}$ is an outward unit vector normal to the object contour, $\vec{H}_i = H_0 exp(-j\vec{k}_0\cdot\vec{r}')\hat{x}$, and $G(|\vec{r}-\vec{r}'|)$ is a two–dimensional Green's function. Whereas the scattered field for a dielectric object satisfying the Born approximation is given as [2]

$$\vec{E}_s^d(x,z=\pm d,\vec{k}_0)=\int k_0^2[\epsilon_r(\vec{r}')-1]\vec{E}_i G(|\vec{r}-\vec{r}'|)d^2r' \tag{2}$$

where $\vec{E}_i = E_0 exp(-j\vec{k}_0\cdot\vec{r}')\hat{y}$, and $\epsilon_r(\vec{r}')$ is the object dielectric constant distribution.

Assuming the polarization state of receiving array in the direction of $\hat{p}$, the scattered field recorded by a linear array at $z=d$ or $z=-d$ obtained from eq.(1) becomes

$$U_s^c(x,z=\pm d,\vec{k}_0)=-j\omega\mu_0 H_0\iint O^c(\vec{r}')e^{-j\vec{k}_0\cdot\vec{r}'}G(|\vec{r}-\vec{r}'|)d^2r' \tag{3}$$

where

$$O^c(\vec{r}')=\hat{p}\cdot(2\hat{n}\times\hat{x})\delta(C(\vec{r}')) \tag{4}$$

is defined as the object function of perfectly conducting object which is related to the object shape, and $\delta(\cdot)$ is an one–dimensional Dirac–delta function with its argument defined as $C(\vec{r}')=0$ as $\vec{r}'\in C_{ill}$ and $\neq 0$ elsewhere to reduce the surface integral in eq.(3) to the line integral in eq.(1).

Similarly eq.(5) becomes

$$U_s^d(x,z=\pm d,\vec{k}_0)=k_0^2 E_0\iint O^d(\vec{r}')e^{-j\vec{k}_0\cdot\vec{r}'}G(|\vec{r}-\vec{r}'|)d^2r' \tag{5}$$

where

$$O^d(\vec{r}')=\hat{p}\cdot\hat{y}[\epsilon_r(\vec{r}')-1] \tag{6}$$

90CH2776-3/0000-1028 $1.00 ©1990 IEEE

is defined as the object function of scattering dielectric object which is related to the object dielectric constant distribution.

By one–dimensional Fourier transforming the resulting expression of $U_s^c(x, z=\pm d, \vec{k}_0)$ and $U_s^d(x, z=\pm d, \vec{k}_0)$ in the x–direction, one can obtain

$$\tilde{U}_s^c(k_x, z=\pm d, \vec{k}_0)=\frac{-\omega\mu_0 H_0}{2k_z} e^{-jk_z d}\tilde{O}^c(k_x-k_{x0}, \pm k_z-k_{z0}) \tag{7}$$

and

$$\tilde{U}_s^d(k_x, z=\pm d, \vec{k}_0)=\frac{-jk_0^2 E_0}{2k_z} e^{-jk_z d}\tilde{O}^d(k_x-k_{x0}, \pm k_z-k_{z0}) \tag{8}$$

Equations (7) and (8) show that, except for the scaling factors, one–dimensional Fourier transformation of the scattering field recorded by a linear array located at $z=d$ or $z=-d$ (i.e., forward or backward scattering arrangement) yields a semi–circular slice centered at $(-k_{x0}, -k_{z0})$ with radius k_0 in the two–dimensional Fourier space $\tilde{O}(k_x, k_z)$ of the object function as shown in Fig.2(a) and (b). These are known as the Fourier diffraction projection theorems for image reconstruction of perfectly conducting and dielectric scattering objects.

In order to reconstruct the image of object function with high resolution from the acquired Fourier space data using two–dimensional Fourier inversion, additional degrees of freedom to acquire the Fourier space data are required. Two effective approaches are described in the following numerical simulation.

III. Numerical Simulation

Numerical results of a perfectly conducting cylinder with radius 15cm located at z=30cm or –30cm from a 384cm long linear receiving array are shown in Fig.3. In the first approach using angular diversity techinique in forward scattering arrangement the acquired Fourier space data, as shown in Fig.3(a), are calculated at 256 sample points on the linear array with a total of 128 equally spaced views over 360° at 10GHz. The polarization state of receiving antennas are in the y–direction. Whereas in the second approach using frequency diversity technique the backward scattered field, as shown in Fig.3(c), are calculated at 256 sample points with four orthogonal views and frequency stepped from 5GHz to 10GHz in 32 steps. Images reconstructed from the acquired Fourier space data using two–dimensional Fourier inversion shown in Figs.3(b) and (d) are in good agreement with the scattering object geometry. The images obtained in both approaches represent the shape of scattering perfectly conducting object.

Numerical results of a homogeneous dielectric cylinder of ϵ_r=1.01 with the same scattering parameters as those for the perfectly conducting cylinder case are shown in Fig.4. Image shown in Fig.4(c) obtained from the first approach shows the dielectric constant distribution of the test object. Since a bandpass version of object Fourier space data is acquired in the second approach, the image shown in Fig.4(d) inherently gives the "edge" information of the test dielectric object. As shown in Fig.4, these two approaches yield different feature information of the test dielectric object, and they are useful in the application of nondestructive evaluation.

References
[1] R.F. Harrington, *Time–Harmonic Electromagnetic Fields*, McGraw-Hill, New York, 1961.
[2] E. Wolf, "Three–dimensional Structure Determination of Semi-Transparent Objects from Holographic Data," *Optics Communications*, Vol. 1, No. 4, pp. 153–156, Sep./Oct. 1969.

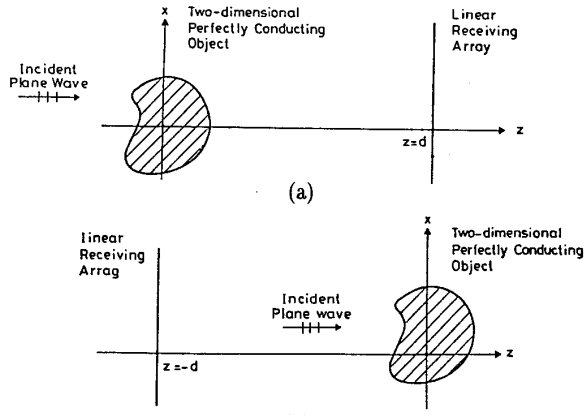

Fig.1 (a) Forward and (b) backward scattering geometries.

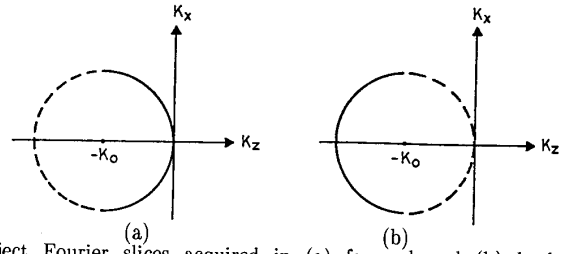

Fig.2 Object Fourier slices acquired in (a) forward and (b) backward scattering arrangements with single frequency (wavenumber k_0) plane wave illumination.

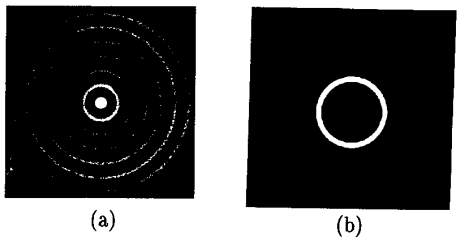

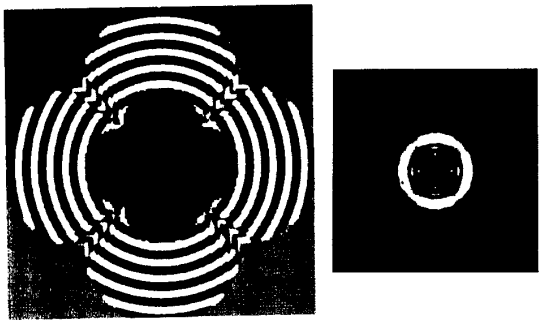

(c) (d)

Fig.3 Simulation results of perfectly conducting cylinder. (a) Fourier space data and (b) reconstructed image using the first approach, (c) Fourier space data and (d) reconstructed image using the second approach.

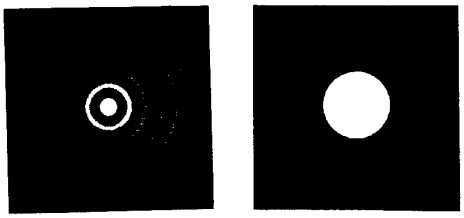

(a) (b)

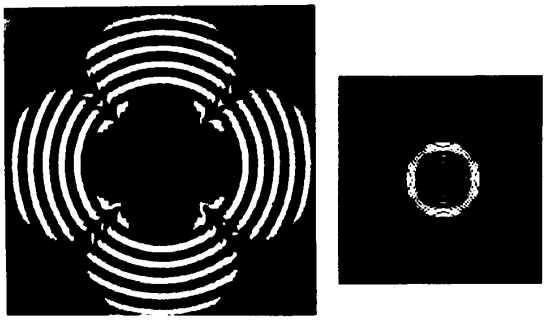

(c) (d)

Fig.4 Simulation results of dielectric cylinder. (a) Fourier space data and (b) reconstructed image using the first approach, (c) Fourier space data and (d) reconstructed image using the second approach.